Comparative Thermodynamic Analysis of DNA−Protein Interactions Using Surface Plasmon Resonance and Fluorescence Correlation Spectroscopy†

Frank Schubert,*,‡ Heiko Zettl,‡ Wolfgang Häfner,‡ Gerhard Krauss,§ and Georg Krausch‡

Physikalische Chemie II and Laboratorium für Biochemie, Universität Bayreuth, Universitätsstrasse 30, 95447 Bayreuth, Germany

Received January 9, 2003; Revised Manuscript Received July 8, 2003

ABSTRACT: We report a kinetic and thermodynamic analysis of interactions between ssDNA and replication protein A (RPA) using surface plasmon resonance (SPR) and fluorescence correlation spectroscopy (FCS) at variable temperature. The two methods yield different values for the Gibbs free energy but nearly the same value for the reaction enthalpy of ssDNA−RPA complex formation. The Gibbs free energy was determined by SPR and FCS to be −62.6 and −54.7 kJ/mol, respectively. The values for the reaction enthalpy are −64.4 and −66.5 kJ/mol. It is concluded that the difference in Gibbs free energy measured by the two methods is due to different reaction entropies. The entropic contribution to the free energy at 25 °C is −1.8 kJ/mol for SPR and −11.8 kJ/mol for FCS. In SPR, the reaction is restricted to two dimensions because of immobilization of the DNA molecules to the sensor surface. In contrast, FCS is able to follow complex formation without spatial restrictions. In consequence, the reaction entropy determined from SPR experiments is lower than for FCS experiments.

Methods for the characterization of DNA−protein interactions are of great importance in the study of cellular processes, such as DNA replication and repair. Surface plasmon resonance (SPR)[1] and fluorescence correlation spectroscopy (FCS) have emerged as a powerful alternative to classical biochemical methods for the characterization of ligand−receptor binding in biomolecular systems. A key advantage of the two methods, as compared to conventional methods, lies in the speed and simplicity of the analysis. An interesting phenomenon concerning SPR and FCS is that the two methods often yield different values for the equilibrium constants. To explain this, one has to take a closer look at the thermodynamics of biomolecular interactions using SPR and FCS.

SPR is a method to monitor the interactions between biomolecules. It is an optical technique that uses the evanescent wave phenomenon to measure changes in the refractive index close to a sensor surface. The binding between an analyte in solution and a receptor immobilized on the sensor surface results in a change in the refractive index (*1*, *2*). Continuous monitoring of the SPR signal allows the kinetics of binding to be followed in real time, and the amount of bound ligand and the association and dissociation rates can be measured with high precision. The main advantage of SPR is that no particular property (e.g., fluorescence or radioactive label) of either of the interacting molecules is required. It is assumed that the rate constants determined by SPR reflect the true association and dissociation rates of the complex formation. This, however, might be not the case, as the immobilization of one of the reaction partners might well influence the kinetics of the binding process.

FCS was developed in the early 1970s by Elson et. al (*3*−*5*). It measures mean diffusion times and concentrations of a fluorophore by evaluating fluctuations in the fluorescence intensity. The latter originate from the Brownian motion of the fluorophore through a small volume defined by the focus of the excitation laser beam. The intensity fluctuations depend on the speed of the fluorophore moving through the focus. To follow a biochemical reaction by FCS, typically one of the reactions partners is labeled by a fluorophore. As the size of the reactant increases on complex formation, its characteristic diffusion time will increase as well. Therefore, FCS can be used to follow the binding process via determination of the diffusion times. A major advantage of this method is that the molecules are freely moving in solution, so the system is not influenced by a surface. To distinguish between the free reactant and the complex, the diffusion time has to increase at least by a factor of 2 upon binding (*6*, *7*). Care has to be taken to avoid photobleaching of the fluorophore, which sets an upper limit for the diffusion times that can be accurately determined by this technique. Moreover, the quantum efficiency of the fluorophore may change upon binding.

In the present study, we have used SPR and FCS to systematically compare the kinetic and thermodynamic data

† These studies were supported by the Deutsche Forschungsgemeinschaft (Grant DFG Kr1369/11).

* To whom correspondence should be addressed. Phone: +49 (0)-921-552753. Fax: +49 (0)921-552059. E-mail: frank.schubert@uni-bayreuth.de.

‡ Physikalische Chemie II.

§ Laboratorium für Biochemie.

[1] Abbreviations: ssDNA, single-stranded DNA; RPA (recombinant) human replication protein A; SPR, surface plasmon resonance; FCS, fluorescence correlation spectroscopy; NER, nucleotide excision repair; ITC, isothermal titration calorimetry; DSC, differential scanning calorimetry; SDS, sodium dodecyl sulfate; PAGE, polyacrylamide gel electrophoresis; HEPES, *N*-2-hydroxyethylpiperazine-*N*′-2-ethanesulfonic acid; DTT, dithiothreitol; HeNe, helium−neon.

10.1021/bi034033d CCC: $25.00
Published on Web 08/06/2003

obtained for the interaction between human replication protein A (RPA; also known as human single-stranded DNA binding protein) and single-stranded DNA. This system is well-characterized and therefore seems suitable for a comparative model study.

RPA is a heterotrimeric protein containing subunits of 70, 32, and 14 kDa. It is involved in replication and recombination processes and participates in the regulation of transcription (*8*, *9*). An essential role of RPA has been demonstrated for nucleotide excision repair (NER), a pathway that removes a variety of major DNA lesions including photoproducts, adducts of carcinogens, and cisplatin (*10*−*13*). By its DNA binding properties, RPA can be classified as a single-stranded DNA binding protein. It binds with high affinity and low sequence specificity to single-stranded DNA (*14*, *15*). In addition, RPA has been shown to bind with high affinity to DNA lesions that cause a distortion of the DNA. Its affinity for damaged sites on double-stranded DNA is by more than 1 order of magnitude higher than for undamaged double-stranded DNA (*16*). Since the chemical nature of the DNA lesions recognized by RPA is diverse, it is believed that RPA binds to unpaired regions created at the sites of DNA damage. The stronger binding of RPA to damaged versus undamaged DNA suggests that RPA participates in the damage recognition step in NER.

DNA binding domains have been identified on the 70 and 32 kDa subunits of RPA, although most of the DNA contacts appear to be mediated by the 70 kDa subunit. Cross-linking experiments have identified a binding site for damaged DNA on this subunit (*17*). Furthermore, X-ray crystallography of a complex between a fragment of the 70 kDa subunit and (dC)8 has revealed details of the binding site for single-stranded DNA. The DNA is bound in a shallow groove containing several aromatic residues and a surplus of positive charges (*18*).

The kinetics of ssDNA−RPA interactions have been investigated earlier by SPR (*19*) and stopped-flow kinetic analysis (*20*, *21*) but only at a single distinct temperature. Temperature-dependent SPR experiments have been reported for various systems (*22*−*26*) but not for the system studied here. Earlier FCS measurements on the kinetics of DNA−protein interactions were in close agreement to classical biochemical methods (*27*), but thermodynamic experiments are not reported. Compared to classical thermodynamic methods such as isothermal titration calorimetry (ITC) and differential scanning calorimetry (DSC), SPR and FCS only require the smallest amounts of DNA and protein.

In this study, we obtained kinetic and thermodynamic data of ssDNA−RPA interactions using SPR spectroscopy and FCS at variable temperature. We find distinctly different equilibrium constants from the two different experimental techniques. Our results indicate that this difference is due to differences in the reaction entropy. The latter difference is believed to result from the quite different degrees of freedom for the reactants in SPR (receptor bound to a two-dimensional surface) and FCS (both partners diffusing freely in solution).

MATERIALS AND METHODS

ssDNA and Proteins. A biotinylated 26-mer ssDNA with the sequence 5′-AAG-TAT-TAT-AAT-CAC-TAA-ATA-CGA-AA-3′ was purchased from Interactiva (Ulm, Germany), and CY5-labeled ssDNA of the same sequence was obtained from MWG-Biotech (Ebersberg, Germany). In both cases, the DNA was modified at the 5′ end. RPA was expressed in *Escherichia coli* BL21 (DE3) using the expression vector pET11d-thRPA (a generous gift from M. S. Wold) and purified following the protocol of Henricksen et al. (*28*) through Affigel-Blue (Biorad), hydroxylapatite (Biorad), and anion-exchange chromatography on EMD-TMAE (Merck). RPA eluted from EMD-TMAE at 200 mM KCl at >95% purity as judged by SDS−PAGE and staining with Coomassie Blue. Aliquots containing 10% glycerol were shock-frozen in liquid nitrogen and stored at −78 °C until use (*16*). For a quantitative determination of the DNA binding activity of our RPA preparation, stoichiometric fluorescence titrations of RPA and ssDNA were performed. ssDNA at a concentration of 50 nM was titrated with RPA, and the fraction of active protein was determined from the equivalence point of the titration curve.

Surface Plasmon Resonance. Interactions of RPA with ssDNA were monitored using a surface plasmon resonance biosensor instrument, BIAcore X (Biacore). The biotinylated ssDNA was diluted to 1.5 nM in buffer containing 10 mM sodium acetate, pH 4.8, and 1.0 M NaCl and manually injected at a flow rate of 5 μL min^{-1} onto an immobilized streptavidin surface of the BIAcore sensor chip. The second flow cell was left underivatized to correct for refractive index changes, nonspecific binding, and instrument drift. Proteins were diluted into running buffer containing 10 mM HEPES, pH 7.4, 150 mM NaCl, 2 mM MgCl2, 0.005% Polysorbate-20, and 1 mM DTT. The flow rate during the experiments was 10 μL min^{-1}. Following RPA binding, regeneration was performed with a 30 s injection of 0.25% SDS in buffer. All sensorgrams were analyzed for bulk drift and mass transport influenced kinetics. The temperature was controlled using Peltier elements to maintain a constant temperature at the sensor chip surface; the deviation from the preset temperature was around 0.1 °C. Each experiment was repeated at least three times to ensure reproducibility.

Data Analysis for Surface Plasmon Resonance. The procedures for the analysis were essentially the same as described by the manufacturer (*29*). Both association and dissociation rate constants can be extrapolated from the data in the sensorgrams (*30*, *31*). The ssDNA−RPA interaction data were fit to a simple reversible reaction mechanism

$$\mathrm{A} + \mathrm{B} \underset{k_\mathrm{d}}{\overset{k_\mathrm{a}}{\rightleftharpoons}} \mathrm{AB} \qquad (1)$$

A represents the RPA in solution, and B stands for the immobilized ssDNA. k_a and k_d are the association and dissociation rate constants, respectively. The two rate constants were obtained by nonlinear fitting of the sensorgram data using the BIAevaluation 3.0 software supplied by BIAcore. The dissociation rate constant is derived using the equation

$$R_t = R_{t_0} \mathrm{e}^{-k_\mathrm{d}(t-t_0)} \qquad (2)$$

where R_t is the response at time t, and R_{t_0} is the amplitude of the response at the end of the injection. The association rate constant k_a can be derived from the measured k_d values, using

$$R_t = \frac{k_a[A]R_{max}}{k_a[A] + k_d}(1 - e^{-(k_a[A]+k_d)(t-t_0)}) \quad (3)$$

where [A] represents the concentration of the analyte (in this case RPA), and R_{max} represents the maximum binding capacity of the surface.

To test whether the assumption of a single-exponential model for the binding between ssDNA and protein is justified, all SPR data were fitted using a double-exponential model as well. However, *F*-tests of the quality of the different models clearly favor the single-exponential model (eq 1).

The equilibrium constant $K_{D,SPR}$ can be calculated from the ratio of the kinetic rate constants

$$K_{D,SPR} = \frac{k_d}{k_a} \quad (4)$$

Moreover, the equilibrium constants may be determined from biosensor data if the reaction reaches a steady-state response R_{eq} during the association phase. The equilibrium constant can be determined from nonlinear least squares curve fitting of the data to

$$R_{eq} = R_{max}\frac{1}{1 + \frac{K_D}{[A]}} \quad (5)$$

Fluorescence Correlation Spectroscopy. Measurements were made on a ConfoCor 2 FCS instrument (Zeiss, Jena). A HeNe laser with 5 mW power at 633 nm was focused by a water immersion Zeiss C Apochromat 40 × 1.2 objective, and the laser attenuation was set to 0.3%. A 90 μm pinhole was used in the confocal detection channel. The samples were measured in home-built sample chambers with an ~140 μm thick cover slide on the bottom. The focus of the lens was placed ~200 μm above the surface of the cover slide. All experiments were carried out with 1 and 5 nM ssDNA in the same binding buffer as used for the SPR experiments. At the beginning of each experiment, the diffusion time of CY5 was determined by averaging three measurements of 60 s each. The diffusion time of the ssDNA was determined once for each temperature. After filling the chamber with ssDNA−protein solution and an incubation time of ~5 min to reach equilibrium, the autocorrelation functions were recorded for 180 s for each point of the reverse titration.

For temperature control, we used a Peltier element and two PT100 sensors, one placed close to the Peltier element and the other placed near the sample. The deviation from the preset temperature was around 0.1 °C.

Data Analysis for Fluorescence Correlation Spectroscopy. The autocorrelation functions for the titration of ssDNA with RPA were evaluated by a homemade routine performing least-squares fits according to the extended autocorrelation function for *K* different particles including triplet states (*32*):

$$G(\tau) = \frac{1 + \frac{T}{1-T}e^{-\tau/\tau_{tr}}}{N}\sum_{i=1}^{K}\frac{\phi_i}{1 + \frac{\tau}{\tau_i}}\frac{1}{\sqrt{1 + \frac{\tau}{S^2\tau_i}}} + 1 \quad (6)$$

where *T* is the fraction of fluorescent molecules that are in the triplet state with the lifetime τ_{tr}, *N* is the average number of fluorescent molecules in the sample volume, ϕ_i is the fraction of the *i*th component, and *S* is the structure parameter that describes the shape of the sample volume. The characteristic diffusion time of the *i*th component τ_i is the mean time a particle spends in the illuminated volume. This treatment is only valid if the quantum yield and the extinction coefficient of the fluorophore do not change upon binding. The diffusion time τ_i is related to the diffusion coefficient D_i by the equation

$$D_i = \frac{w_{xy}^2}{4\tau_i} \quad (7)$$

where w_{xy} represents the waist radius of the laser beam in the *xy*-plane perpendicular to the optical axis.

The autocorrelation functions for the complex formation were fitted using eq 6 for two particles ($K = 2$) (i.e., ssDNA molecules and ssDNA−RPA complexes). From measurements of CY5, the structure parameter *S* was determined for each experiment. The diffusion time τ_1 was obtained from measurements of the free ssDNA in the absence of protein for each experiment. At saturating protein concentrations, the diffusion time τ_2 of the protein−DNA complex could be determined. The degree of binding $\theta = \phi_2 = 1 - \phi_1$ remained the only unknown parameter and was determined from eq 6 at each titration point. The resulting θ values were fitted to

$$\theta = \frac{\alpha - \sqrt{\alpha^2 - 4[A][B]}}{2[B]} \quad (8)$$

with $\alpha = [A] + [B] + K_{D,FCS}$, where [A] is the RPA concentration, [B] is the concentration of ssDNA, and $K_{D,FCS}$ is the equilibrium constant for the dissociation.

Thermodynamics. The Gibbs free energy change ΔG for a reaction is related to the equilibrium dissociation constant by

$$\Delta G = -RT \ln K_A = RT \ln K_D \quad (9)$$

R is the gas constant, and *T* is the absolute temperature. A noncalorimetric approach to determine the reaction enthalpy ΔH for a binding reaction is the van't Hoff analysis. A key assumption in using the van't Hoff relationship is that the binding reaction involves a single equilibrium throughout the temperature range studied. For protein reactants, it may be necessary to establish that they do not aggregate or change conformation over the temperature range studied. For a simple equilibrium reaction, the van't Hoff enthalpy change is calculated from the temperature dependence of a given equilibrium dissociation constant. The relationship between the equilibrium constant and the reaction enthalpy ΔH, and the reaction entropy ΔS, is the van't Hoff expression

$$\ln K_D = \frac{\Delta H}{R}\frac{1}{T} - \frac{\Delta S}{R} \quad (10)$$

The slope of $\ln K_D$ versus $1/T$ provides $\Delta H/R$, from which the enthalpy can be calculated.

The temperature-dependent measurements can also be used to obtain the activation energy E_A for the association and

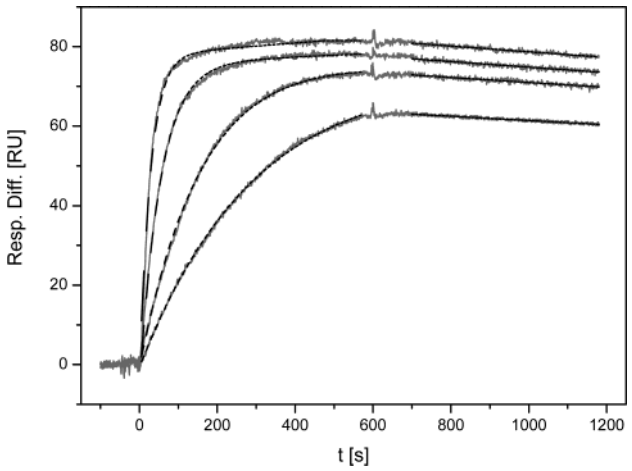

FIGURE 1: SPR sensorgrams showing the interactions between RPA and ssDNA at RPA concentrations of 0.3, 0.5, 1.5, and 3.0 nM at 25 °C. Binding was allowed to proceed for 600 s of the association phase followed by 600 s of running buffer injection period for dissociation. All curves are corrected for bulk shift using an underivatized cell. The baseline drift corrected fits for the dissociation and association phase are shown in the plot. A value of 1.05 ± 0.08 × 10^{-11} M was determined for $K_{D,SPR}$.

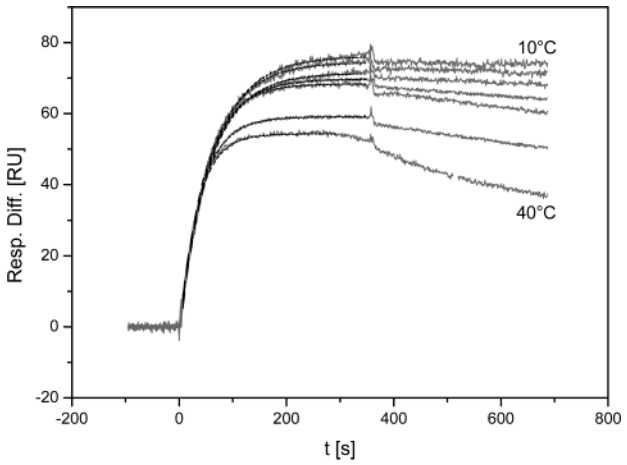

FIGURE 2: Sensorgrams and fits for association for ssDNA−RPA interactions at 10, 15, 20, 25, 30, 35, and 40 °C. The RPA concentration was 1.7 nM. Binding was allowed to proceed for 360 s of association phase followed by 360 s of a running buffer injection period for dissociation. A decrease in the response with increasing temperature is due to the temperature dependence of the refractive index; the rate of dissociation becomes faster with increasing temperature.

dissociation phase using the Arrhenius relationship

$$\ln k = \ln k_0 - \frac{E_A}{R}\frac{1}{T} \qquad (11)$$

where k is an apparent rate constant, and k_0 is the frequency factor for the given reaction.

RESULTS

It is known that RPA binds to ssDNA in different ways, depending on the length of the DNA strand (*33*). Only ssDNA molecules longer than 15−16 nucleotides are efficiently bound by RPA, and the size of the binding site on the ssDNA strand is between 8 and 10 nucleotides. Therefore, we have chosen a 26-mer oligonucleotide to avoid the binding of more than one RPA per DNA. The same oligonucleotide was used for both SPR and FCS experiments. Moreover, we have performed SPR experiments with a 15-mer oligonucleotide to compare if there is a difference in RPA binding.

Kinetic and Thermodynamic Data Obtained by SPR. Kinetic analysis of RPA binding required a biosensor surface derivatized with low levels of ssDNA to avoid mass-transfer effects and to approach equilibrium binding (Figure 1). Analysis of the dissociation data revealed a dissociation rate constant of 1.31 × 10^{-4} s^{-1} at 25 °C. Analysis of the association data for protein concentrations ranging from 0.2 to 3 nM resulted in an association rate constant of 1.25 × 10^7 M^{-1} s^{-1} at 25 °C. From the rate constants, an equilibrium constant $K_{D,SPR}$ = 1.05 × 10^{-11} M was calculated.

Evaluating the temperature-dependent measurements (Figure 2) in the same way, we obtained the values given in Table 1. The k_a for the complex formation ranged from 0.96 to 1.74 × 10^7 M^{-1} s^{-1}, and the k_d ranged from 0.26 to 8.45 × 10^{-4} s^{-1}. Therefore, the $K_{D,SPR}$ values were estimated to be 0.27−4.86 × 10^{-11} M. Performing a van't Hoff analysis (Figure 3A), we obtained a value for the reaction enthalpy $\Delta H = -64.4 \pm 5.5$ kJ mol^{-1}. From the Arrhenius plot shown in Figure 3B (eq 11), we obtain an activation energy E_A = 14.43 ± 1.49 kJ mol^{-1} for the association reaction, indicating that a large amount of energy has to be expended for binding to occur. The activation energy for the dissociation reaction is 78.93 ± 5.38 kJ mol^{-1}. The difference between the activation energies for dissociation and association is equal to the reaction enthalpy. This yields a value for the reaction enthalpy of 64.50 ± 5.58 kJ mol^{-1}, which is in good agreement with the value of the van't Hoff analysis.

Table 1: Values of K_a, k_d, and $K_{D,SPR}$ for the ssDNA−RPA Interactions at Various Temperatures Obtained from SPR Experiments

T [°C]	k_a [M^{-1} s^{-1}]	k_d [s^{-1}]	$K_{D,SPR}$ [M]
10	9.56 ± 0.25 × 10^6	2.55 ± 0.33 × 10^{-5}	2.66 ± 0.36 × 10^{-12}
15	1.05 ± 0.03 × 10^7	7.27 ± 0.30 × 10^{-5}	6.90 ± 0.33 × 10^{-12}
20	1.08 ± 0.02 × 10^7	9.46 ± 0.59 × 10^{-5}	8.78 ± 0.56 × 10^{-12}
25	1.25 ± 0.07 × 10^7	1.31 ± 0.07 × 10^{-4}	1.05 ± 0.08 × 10^{-11}
30	1.34 ± 0.08 × 10^7	2.82 ± 0.08 × 10^{-4}	2.11 ± 0.14 × 10^{-11}
35	1.52 ± 0.06 × 10^7	3.97 ± 0.26 × 10^{-4}	2.61 ± 0.20 × 10^{-11}
40	1.74 ± 0.04 × 10^7	8.45 ± 0.53 × 10^{-4}	4.86 ± 0.33 × 10^{-11}

Thermodynamic Data Obtained by FCS. The binding of RPA to ssDNA was studied by FCS. Normalized autocorrelation curves are shown in Figure 4. The diffusion times of free and protein-bound ssDNA were determined from the autocorrelation functions with no protein and excess of protein in the solution from the fit to a one component model (eq 6, $\theta = 0$ or $\theta = 1$). From this, we obtained a diffusion time τ_{DNA} = 152.1 ± 2.4 μs for the free DNA and $\tau_{complex}$ = 450.8 ± 5.2 μs for the complex (both values taken at 25 °C). With increasing temperature, we found a decrease in the diffusion times that can be attributed to viscosity changes of the aqueous solution (*34*). The progress of complex formation at 25 °C is shown in Figure 5. The diffusion times were obtained by least-squares fits using eq 6 for a single particle ($K = 1$). It is clearly seen that the mean diffusion time increases with increasing RPA concentration and reaches a constant value, indicating the formation of ssDNA−RPA complexes.

The diffusion coefficients D_i of CY5, ssDNA, and the ssDNA−RPA complex, respectively, were calculated from

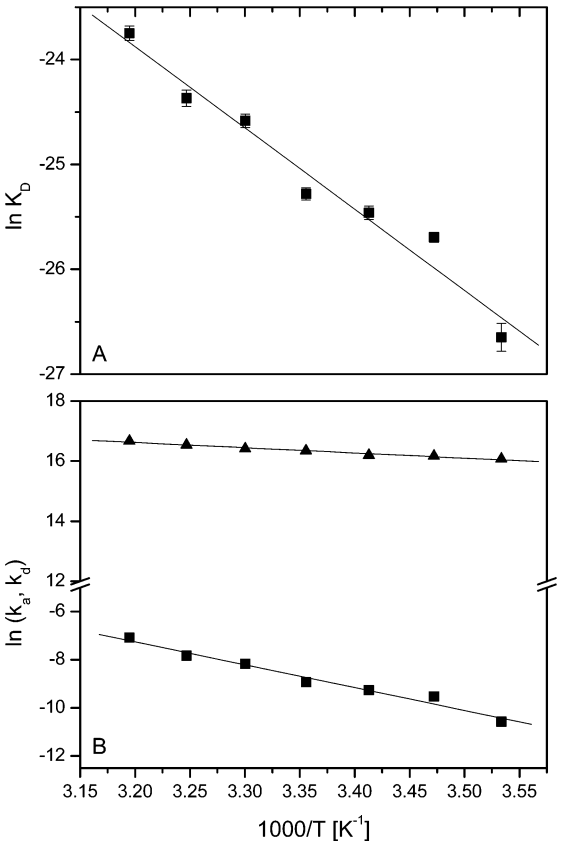

FIGURE 3: (A) van't Hoff plot of the ssDNA−RPA interaction obtained from SPR measurements. Linear fit to eq 10 gave a value for ΔH of -64.4 ± 5.5 kJ mol^{-1}. (B) Arrhenius plot for the association (▲) and dissociation (■) reaction of RPA with ssDNA obtained from SPR experiments. Error bars have been omitted because they are smaller than the symbols used.

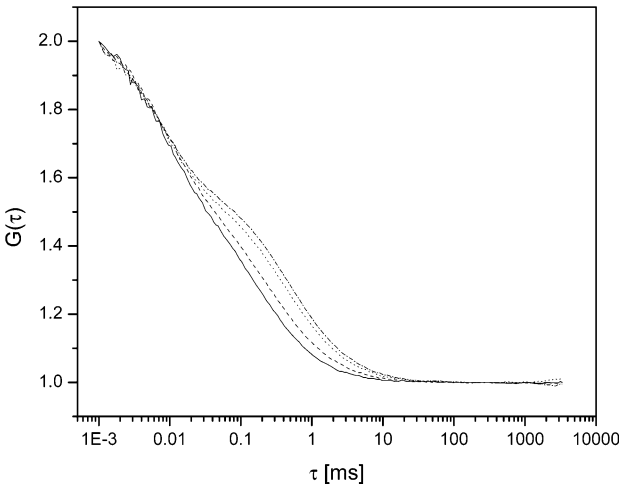

FIGURE 4: Normalized autocorrelation functions for different RPA concentrations at 25 °C. The percentage of the complex was determined by a two component fit to each function. Curves for 0% (solid line), 40% (dashed line), 81% (dotted line), and 100% (dash−dotted line) of the ssDNA−RPA complex are shown. An increase in diffusion time with increasing complex fraction can clearly be seen.

the diffusion times τ_i using eq 7. The dynamics of molecules in liquids are not well-understood, and numerous theoretical models are found in the literature. A simple approach is to assume an Arrhenius behavior of the temperature dependence of the diffusion coefficient (*35*) (i.e., $D = D_0 e^{-E_A/RT}$) (Figure 6), with an activation energy E_A that is equal to the enthalpy barrier to molecular migration.

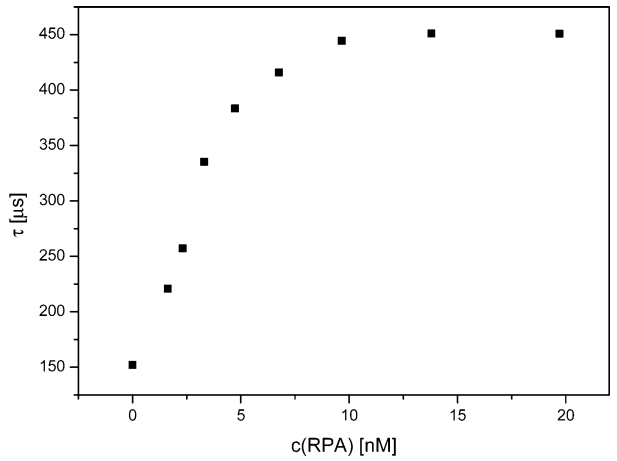

FIGURE 5: Progress of complex formation at 25 °C as a function of RPA concentration. The diffusion times were obtained by fitting eq 6 for one particle ($K = 1$). Error bars have been omitted from the plot because they are smaller than the symbols used.

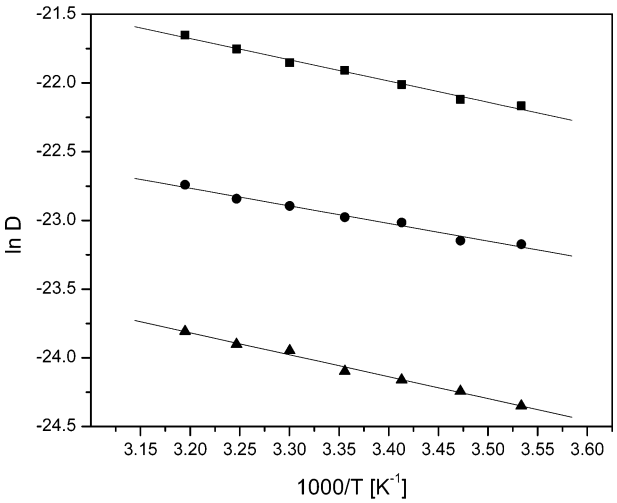

FIGURE 6: Temperature dependence of the diffusion coefficient for CY5 (■), ssDNA (●), and the ssDNA−RPA complex (▲) according to Arrhenius behavior. The diffusion coefficients were calculated using eq 7. Error bars have been omitted from the plot because they are smaller than the symbols used.

Titration curves can be obtained from the FCS curves by fitting a two species model (eq 6) with fixed diffusion times to the autocorrelation function at each titration point. A fit using eq 8 gave a value of 2.61×10^{-10} M for the dissociation constant at 25 °C.

Titration curves derived from autocorrelation functions at various temperatures are depicted in Figure 7A,B. The measurements were performed at DNA concentrations of 1 nM (Figure 7A) and 5 nM (Figure 7B). Unfortunately, it was not possible to obtain reliable data for temperatures above 25 °C at 1 nM DNA. We assume that this is due to instabilities of the dye and the protein in very dilute solutions. Nevertheless, the equilibrium constants obtained from both experiments are the same within the experimental error. The $K_{D,FCS}$ values obtained from these titration curves ranged from 0.64 to 8.52×10^{-10} M in the temperature range studied. Performing a van't Hoff analysis (Figure 8), we obtained a value for the enthalpy of the reaction ΔH of -66.5 ± 8.9 kJ mol^{-1}.

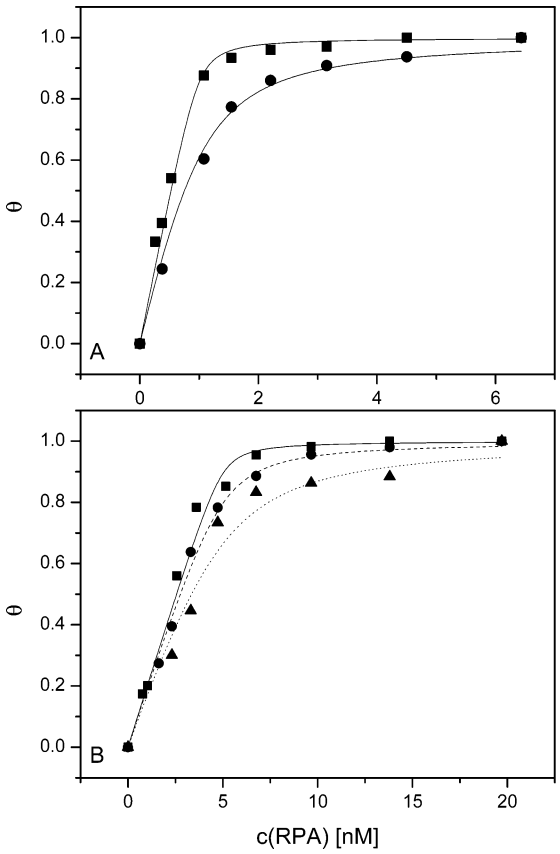

FIGURE 7: (A) Titration curves derived from the autocorrelation functions for a DNA concentration of 1 nM at 10 °C (■) and 25 °C (●). We were not able to obtain reliable data above 25 °C. (B) Titration curves derived from the autocorrelation functions for a DNA concentration of 5 nM at 10 °C (■), 25 °C (●), and 40 °C (▲). The values for the equilibrium constants are, within the range of error, the same for the two different DNA concentrations. Error bars have been omitted from the plot because they are smaller than the symbols used.

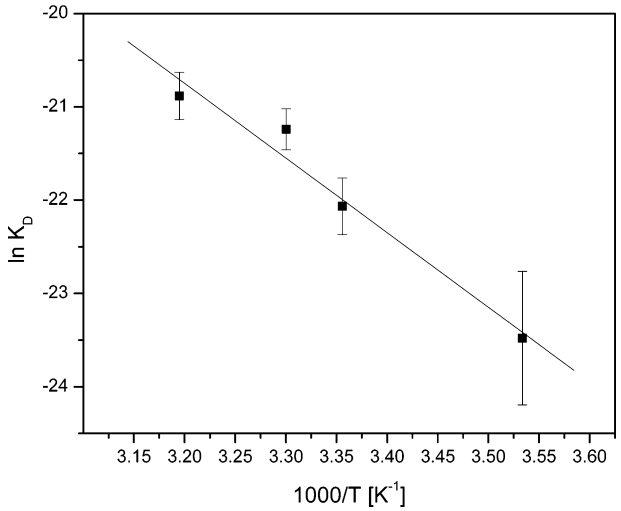

FIGURE 8: van't Hoff plot of the ssDNA−RPA interaction obtained from titration curves at 5 nM DNA concentration. Linear fit to eq 10 gave a value for ΔH of -66.5 ± 8.9 kJ mol^{-1}.

The equilibrium constants and thermodynamic parameters of ssDNA−RPA interactions at 25 °C obtained by SPR and FCS are summarized in Table 2. Within the experimental error, both methods yield the same values of the reaction enthalpy.

Table 2: Equilibrium Constants and Thermodynamic Parameters of ssDNA−RPA Interactions at 25 °C Obtained from SPR and FCS Experiments

method	K_D [M]	ΔG [kJ/mol]	ΔH [kJ/mol]	$T\Delta S$ [kJ/mol]
SPR	$1.05 \pm 0.08 \times 10^{-11}$	-62.6 ± 0.19	-64.4 ± 5.5	-1.8
FCS	$2.61 \pm 0.80 \times 10^{-10}$	-54.7 ± 0.75	-66.5 ± 8.9	-11.8

DISCUSSION AND CONCLUSION

The application of SPR and FCS to analyzing the binding of RPA to ssDNA yields information about the kinetics and thermodynamics. No modification of the protein is required, and biotinylated and fluorescently labeled DNA strands are available from commercial sources. Salt concentration, pH, and temperature can be varied over a wide range. This has been demonstrated here by measuring the kinetics and thermodynamics in a temperature range from 10 to 40 °C.

A number of studies have been published utilizing SPR to study the kinetics and thermodynamics of interactions between various proteins, including RPA, and DNA (*19*, *22*, *36*−*40*). The kinetic data we obtained by SPR for the formation of a ssDNA−RPA complex are comparable to values reported in the literature (*19*). We found values for the rate constants and the equilibrium constant that are slightly deviating from the reported values for a 70-mer ssDNA. This length difference may well be the reason for the discrepancy, as the binding process is known to depend on the length of the DNA. To the best of our knowledge, FCS has not been used previously to obtain equilibrium constants at different temperatures. In the work reported here, we have demonstrated how temperature-dependent SPR and FCS measurements can be performed and evaluated to determine the thermodynamic data of DNA−protein interactions.

The SPR experiments might be affected by the fact that the DNA is immobilized on the surface of the sensor chip; thus, the rate constants obtained might not be the true association and dissociation rates. To obtain values that are not influenced by the surface, we need to perform competitive measurements in future work. This allows us to determine the affinity in solution so it is possible to compare the true equilibrium constants with the results from FCS experiments.

In our FCS experiments, the quantum efficiency of the dye was not influenced by the binding process. Previous experiments showed that the binding of DNA to RPA is not altered significantly by attaching a label to the DNA (*16*). It was found that the equilibrium constant remained the same within the experimental error for labeled and unlabeled DNA. Moreover, there was no interaction between RPA and free CY5. Therefore, significant deviations due to labeling can be ruled out in our experiments. The fluorescence emission rate per dye molecule increased by approximately 50% when the temperature was decreased from 40 to 10 °C. This tendency has also been observed by Widengren and Schwille (*34*). We note, however, that the data analysis described above is not influenced by this effect, as long as the intensity of the signal is sufficiently high and as long as the data set for each temperature is evaluated separately. Photobleaching occurred at laser attenuation above 0.7%; therefore, we performed our experiments below this threshold value. Photobleaching also occurred at RPA concentrations above

50 nM, which indicates that a slowly diffusing complex with two or more RPA molecules is formed. It is known that RPA forms dimers or trimers upon binding to DNA (*33*), depending on the length of the DNA.

The equilibrium constant $K_{D,FCS}$ for the binding obtained by FCS is by a factor of 20−25 higher than the value obtained by SPR, depending on the temperature. This was verified by performing the FCS experiments at lower DNA concentrations. In addition to reverse titrations, we observed also the complex formation by adding protein to ssDNA solutions to ensure that the dissociation and formation processes are not kinetically hindered. The values found by SPR and FCS are in agreement with data published earlier (*16*, *19*); the differences are to be sought in different DNA and buffers used in the experiments. The reaction enthalpy gained by SPR and FCS are the same within the experimental error, and the van't Hoff plots of SPR and FCS data were linear with regression coefficients >0.98.

In this study, we took a closer look at the thermodynamics of ssDNA−RPA interactions using SPR and FCS at variable temperature. We found different values for the Gibbs free energy but nearly the same value for the reaction enthalpy of ssDNA−RPA complex formation. We have clear evidences that the difference in K_D and therefore in Gibbs free energy measured by the two methods is due to different reaction entropies. In SPR, the reaction is restricted to two dimensions because of immobilization of the DNA molecules to the sensor surface. In contrast, FCS is able to follow complex formation without spatial restrictions. In consequence, the reaction in three dimensions is entropically less favorable than the reaction at the solid liquid interface. This might be due to differences in the cratic entropy between the two geometries; however, the role of hydration cannot be assessed by our experiments.

ACKNOWLEDGMENT

The authors thank T. Hey (Universität Bayreuth) for providing the RPA and R. Beinoraviciute-Kellner (Universität Bayreuth) for helpful discussions.

REFERENCES

1. Jönsson, U., Fägerstam, L., Ivarsson, B., Johnsson, B., Karlsson, R., Lundh, K., Löfås, S., Persson, B., Roos, H., Rönnberg, I., Sjölander, S., Stenberg, E., Ståhlberg, R., Urbaniczky, C., Östlin, H., and Malmqvist, M. (1991) *BioTechniques 11*, 620−627.
2. Malmqvist, M. (1993) *Nature 361*, 186−187.
3. Magde, D., Webb, W. W., and Elson, E. (1972) *Phys. Rev. Lett. 29*, 705−708.
4. Elson, E. L., and Magde, D. (1974) *Biopolymers 13*, 1−27.
5. Magde, D., Elson, E. L., and Webb, W. W. (1974) *Biopolymers 13*, 29−61.
6. Meseth, U., Wohland, T., Rigler, R., and Vogel, H. (1999) *Biophys. J. 76*, 1619−1631.
7. *Confocor 2 Applications Handbook* (2001) Carl Zeiss, Jena, Germany.
8. Lao, Y., Chang Geun, L., and Wold, M. S. (1999) *Biochemistry 38*, 3974−3984.
9. Wold, M. S. (1997) *Annu. Rev. Biochem. 66*, 61−92.
10. Burns, J. L., Guzder, S. N., Sung, P., Prakash, S., and Prakash, L. (1996) *J. Biol. Chem. 271*, 11607−11610.
11. Wood, R. D. (1999) *Biochimie 81*, 39−44.
12. Patrick, S. M., and Turchi, J. J. (1999) *J. Biol. Chem. 274*, 14972−14978.
13. Lao, Y., Gomes, X. V., Ren, Y., Taylor, J. S., and Wold, M. S. (2000) *Biochemistry 39*, 850−859.
14. Mitsis, P. G., Kowalczykowski, S. C., and Lehman, I. R. (1993) *Biochemistry 32*, 5257−5266.
15. Kim, C., Paulus, B. F., and Wold, M. S. (1994) *Biochemistry 33*, 14197−14206.
16. Hey, T., Lipps, G., and Krauss, G. (2001) *Biochemistry 40*, 2901−2910.
17. Schweizer, U., Hey, T., Lipps, G., and Krauss, G. (1999) *Nucleic Acids Res. 27*, 3183−3189.
18. Bochkarev, A., Pfuetzner, R. A., Edwards, A. M., and Frappier, L. (1997) *Nature 385*, 176−181.
19. Wang, M., Mahrenholz, A., and Lee, S. H. (2000) *Biochemistry 39*, 6433−6439.
20. Patrick, S. M., and Turchi, J. J. (2001) *J. Biol. Chem. 276*, 22630−22637.
21. Iakoucheva, L. M., Walker, R. K., Van Houten, B., and Ackerman, E. J. (2002) *Biochemistry 41*, 131−143.
22. Seimiya, M., and Kurosawa, Y. (1996) *FEBS Lett. 398*, 279−284.
23. Thomas, C. J., and Surolia, A. (2000) *Arch. Biochem. Biophys. 374*, 8−12.
24. Myszka, D. G. (2000) *Methods Enzymol. 323*, 325−340.
25. Deinum, J., Gustavsson, L., Gyzander, E., Kullman-Magnusson, M., Edström, Å., and Karlsson, R. (2002) *Anal. Biochem. 300*, 152−162.
26. Wang, L., Kumar, A., Boykin, D. W., Bailly, C., and Wilson, W. D. (2002) *J. Mol. Biol. 317*, 361−374.
27. Sevenich, F. W., Langowski, J., Weiss, V., and Rippe, K. (1998) *Nucleic Acids Res. 26*, 1373−1381.
28. Henricksen, L. A., Umbricht, C. B., and Wold, M. S. (1994) *J. Biol. Chem. 269*, 11121−11132.
29. *BIAevaluation 3.0 Software Handbook* (1997) Biacore AB.
30. Karlsson, R., Michaelsson, A., and Mattsson, L. (1991) *J. Immunol. Methods 145*, 229−240.
31. O'Shannessy, D. J., Brigham-Burke, M., Soneson, K. K., Hensley, P., and Brooks, I. (1993) *Anal. Biochem. 212*, 457−468.
32. Widengren, J., Mets, U., and Rigler, R. (1995) *J. Phys. Chem. 99*, 13368−13379.
33. Blackwell, L. J., and Borowiec, J. A. (1994) *Mol. Cell. Biol. 14*, 3993−4001.
34. Widengren, J., and Schwille, P. (2000) *J. Phys. Chem. A 104*, 6416−6428.
35. McCall, D. W., Douglass, D. C., and Anderson, E. W. (1959) *J. Chem. Phys. 31*, 1555−1557.
36. Buckle, M. (2001) *Methods Mol. Biol. 148*, 535−546.
37. Chua, Y. L., Pwee, K. H., Kini, R. M., Leng, C. Y., and Hock, P. K. (2001) *Plant Mol. Biol. 46*, 193−204.
38. Imanishi, M., and Sugiura, Y. (2002) *Biochemistry 41*, 1328−1334.
39. Rüfer, A., Neuenschwander, P. F., and Sauer, B. (2002) *Anal. Biochem. 308*, 90−99.
40. Yang, W., Zeng, W., Zhou, D., and Shi, Y. (2002) *Biochim. Biophys. Acta Proteins Proteom. 1598*, 147−155.

BI034033D